EVIDENCE OF LITHOSPHERIC COOLING PRIOR TO MELT INFILTRATION HISTORY AT THE OMAN PALEO-SPREADING CENTRE (WADI TAYIN MASSIF)

Valentin Basch*,✉, Laura Crispini, Caterina Battifora**** and **Elisabetta Rampone****

* *Istituto Geoscienze e Georisorse, Unità di Pavia, CNR, Pavia, Italy.*
** *Dipartimento di Scienze della Terra, dell'Ambiente e della Vita, Università di Genova, Italy.*
✉ *Corresponding author, email: valentin.basch@gmail.com*

Keywords: *Reactive porous flow; cooling; oceanic lithosphere; geodynamic environment.*

ABSTRACT

The Oman ophiolites offer exceptional exposure of fossil oceanic lithosphere and have been used as a proxy to define the Penrose model of fast-spread oceanic lithosphere. It is composed of several large massifs in which extensive field mapping allowed to reconstruct the position of several paleo-spreading segments. Yet, the geodynamic setting of formation and evolution of this oceanic lithosphere is still debated, between a mid-ocean ridge and back-arc setting. The southern massifs are widely recognized to best expose the primary accretion of the lithosphere, whereas the northern massifs expose a widespread secondary andesitic magmatic phase. To constrain the geodynamic evolution of the Oman oceanic lithosphere, we investigate the processes registered by the upper mantle section from the Wadi Tayin, sampled during the Oman Drilling Project (Holes CM1A and CM2B). We here provide a petrochemical study of spinel harzburgites and pyroxenites sampled within the uppermost mantle, few tens of meters from the Moho Transition Zone. The main processes that we document are: i) the segregation of pyroxenite veins during (reactive) melt percolation at spinel-facies conditions, ii) cooling of the mantle, with partial re-equilibration of the mantle harzburgites and pyroxenites and, iii) reactive porous flow and partial dissolution of mantle pyroxenes. Notably, this chronological evolution involves cooling of the mantle section and incorporation in lithospheric environment prior to the magmatic event leading to percolation of melts through the spinel- to plagioclase-facies lithosphere. Further geochemical studies will allow to constrain the magmatic affinity of percolating melts and the geodynamic setting in which the Oman lithosphere was accreted.

INTRODUCTION

The Oman ophiolites offer exceptional exposure of fossil oceanic lithosphere and have been used as a proxy to define the Penrose model of layered oceanic crust (Anonymous, 1972). It is considered as a fast-spreading analogue, with half-spreading rates of 10 centimetres/year (Rioux et al., 2012; 2013) and displays a complete stratigraphic sequence from ultramafic lithologies to mafic gabbros and its volcano-sedimentary cover (e.g., Boudier and Nicolas, 1985). The Oman ophiolite is composed of several large massifs exposing a more or less complete stratigraphy. Notably, two main magmatic sequences can be distinguished in the extrusive section of the Oman ophiolites (Pearce et al., 1981; Alabaster et al., 1982; Lippard et al., 1986; Beurrier, 1987; Ernewein et al., 1988; Einaudi et al., 2003; Godard et al., 2003; Belgrano et al., 2019). The lower V1 Geotimes extrusive sequence (Pearce et al., 1981; Lippard et al., 1986; Beurrier, 1987; Ernewein et al., 1988; Nicolas et al., 2000; Einaudi et al., 2003; Godard et al., 2003) is exposed along all ophiolitic massifs (Fig. 1a) and shows compositions mostly consistent with tholeiitic basalts, associated with the accretion of the Oman paleo-ridge (94-95 My; e.g., Alabaster et al., 1982; Ernewein et al., 1988; Hacker et al., 1996; Einaudi et al., 2000). The upper V2 sequence is mainly exposed in the northern part of the ophiolite (Pearce et al., 1981; Alabaster et al., 1982; Lippard et al., 1986; Beurrier, 1987; Ernewein et al., 1988; Einaudi et al., 2003; Godard et al., 2003; Belgrano et al., 2019). It is characterized by low-Ti tholeiitic melts, depleted in incompatible trace elements, interpreted either as the first stages of island arc volcanism in an immature arc environment (Pearce et al., 1981; Beurrier et al., 1989; Godard et al., 2003), or as the product of the fluid-enhanced melting of the over-ridden lithosphere during intra-oceanic thrusting of the Oman paleo-ridge (Boudier et al., 1988; Ernewein et al., 1988). At deeper levels within the exposed Oman lithosphere, the numerous intrusions and melt migration structures within the upper mantle have revealed the occurrence of two distinct magmatic suites, between a MORB-type and a depleted andesitic magmatism (Python and Ceuleneer, 2003; Goodenough et al., 2014; Akizawa et al., 2016). Although the context of formation and evolution of the lithosphere is still matter of debate (e.g., MacLeod et al., 2013; Koepke et al., 2021), the differences in parental melt compositions likely reflect an evolution in the geodynamic setting of the Oman ophiolite; the spatial organisation of the Oman intrusives and extrusives thus indicates an increased "arc signature" in the northern massifs, whereas the southern ophiolitic massifs best preserve the decompressional melting-related crustal accretion at the Oman paleo-ridge (e.g., Godard et al., 2003; Goodenough et al., 2014; Belgrano and Diamond, 2019; Guilmette et al., 2021).

Extensive mapping of mantle flow patterns allowed to evidence that crustal accretion is related to mantle diapiric structures representing zones of focussed melt flow and mantle upwelling. The southern ophiolitic massifs (Sumail, Wadi Tayin; see Godard et al., 2000; 2003) display the best exposed examples of such fossil mantle diapirs (Fig. 1), showing kilometre-scale continuous flow structures and radiating peridotite lineations (Rabinowicz et al., 1987; Ceuleneer et al., 1988; 1996; Ceuleneer, 1991; Ceuleneer and Rabinowicz, 1992; Ildefonse et al., 1993; 1995; Nicolas and Boudier, 1995; Boudier et al., 1997; Jousselin and Mainprice, 1998; Godard et al., 2000; Nicolas et al., 2000). These mantle diapirs are the direct expression of asthenospheric upwelling underneath a ridge axis and are topped by a layer of replacive

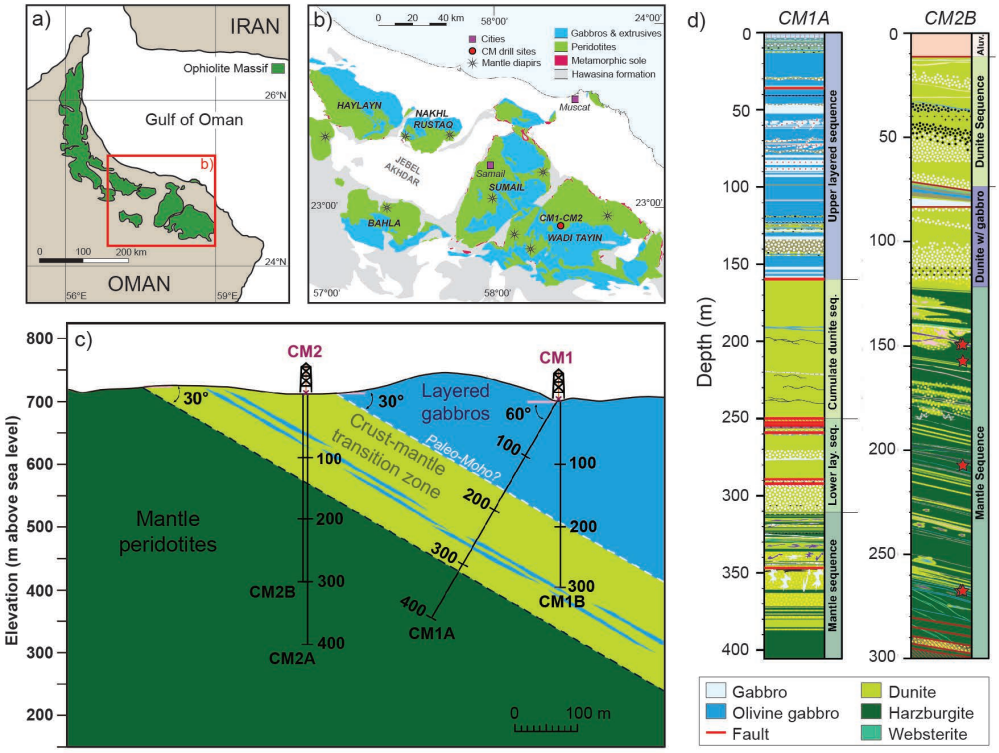

Fig. 1 - a) Structural map of the studied area evidencing the ophiolitic massif in green; b) Geological map of the southern Oman ophiolite, showing the location of the mantle diapirs (after Python and Ceuleneer, 2003) and of drillcores CM1 and CM2 in the Wadi Tayin; c) Representative sketch of a cross-section of the crust-mantle transition zone sampled by the OmanDP CM1 and CM2 drill sites, after Kelemen et al. (2021a; 2021b). Note that the size of the gabbroic lenses found within the crust-mantle transition zone is over-represented and that the location of these lenses is inferred; d) Stratigraphic log of the CM1A and CM2B drillholes, after Kelemen et al. (2021a; 2021b); see online version of the diagram. The studied samples are located with a red star.

dunites indicative of the accumulation of large quantities of melt at the mantle-crust transition (Nicolas and Prinzhofer, 1982; Boudier and Nicolas, 1995; Godard et al., 2000; Jousselin and Nicolas, 2000; Koga et al., 2001; Higgie et al., 2012; Abily and Ceuleneer, 2013; Rospabé et al., 2018). Major attention has been given to the Moho Transition Zone in the southern Oman ophiolites, as an important interface controlling melt evolution and delivery to crustal levels. Conversely, no detailed petrographic and chemical study of the evolution of the upper mantle is available to date. In this framework, the following study aims at documenting the processes registered in the upper mantle harzburgites and pyroxenites, in relation to the spinel-facies evolution of the Oman ophiolite.

GEOLOGICAL SETTING OF THE OMAN DRILLING PROJECT

The Oman ophiolite is an elongated belt exposing 30.000 km^2 of fossil Tethyan oceanic lithosphere along the coastline (Fig. 1a). It formed ~ 95-97 million years ago (e.g., Rioux et al., 2012; 2013) and was followed by its obduction on the Arabian margin ~ 80 million years ago (e.g., Boudier et al., 1988; Montigny et al., 1988). Decades of mapping and sampling of the extrusives and intrusives along the Oman ophiolite (see Godard et al., 2003; Python and Ceuleneer, 2003; Python et al., 2008; Belgrano et al., 2019) revealed that two main magmatic suites contributed to the accretion of the lithosphere: i) a tholeiitic magmatism mostly preserved in the southern ophiolitic massifs and, ii) a depleted andesitic magmatism attributed either to subduction or to water-induced re-melting of the shallow lithosphere (Benoit et al., 1999; Python and Ceuleneer, 2003; Yamasaki et al., 2006; MacLeod et al., 2013; Akizawa et al., 2016; Belgrano et al., 2019; Koepke et al., 2021).

Although the context of formation of the Oman ophiolite is complex and still matter of debate, the exceptional exposure of the complete stratigraphy of this oceanic lithosphere, from the mantle section to the volcano-sedimentary cover, is key to the understanding of the accretion of fast-spread oceanic crust. Accordingly, a complete section of the Wadi Tayin southern ophiolitic massif has recently been sampled during the Oman Drilling Project (OmanDP), from lower crustal gabbros (GT sites) to the crust-mantle transition (CM sites; Fig. 1b) and mantle peridotites (BA sites), for a total of more than 3 kilometres of recovered drillcores. This study focuses on mantle harzburgites from the CM1 and CM2 drillcores (Kelemen et al., 2021a; 2021b) sampled in the northern end of Wadi Zeeb, away from the mantle diapirs reported in the Wadi Tayin area (Fig. 1a; Kelemen et al., 2021a; 2021b). They respectively provide 400m and 300m cores across the crust-mantle transition zone, from the lowermost layered gabbros to the uppermost mantle peridotites (Fig. 1c).

CM1A drill site has been implemented within the Wadi Tayin layered gabbros with a dip of 60°, allowing for sampling roughly perpendicular to the stratigraphy and structure of the ophiolitic massif (Fig. 1c). This core recovered 160 m of layered gabbros, 150 m of massive dunites before transitioning to 90 m of alternating dunite lenses and mantle harzburgites (Fig. 1d). CM2B drill site has been positioned directly within the dunitic transition zone and penetrated the crust-mantle boundary vertically (Fig. 1c). It recovered a similar structure to the other core, with 120 m of massive dunites and minor gabbroic sills overlying a 180 m mantle sequence characterized by alternation between dunite lenses and mantle harzburgites (Fig. 1d).

SAMPLING AND PETROGRAPHY

The recovered upper mantle section of the Wadi Tayin ophiolitic massif (~ 90m in CM1A and ~180m in CM2B; Fig. 1d) is composed of an alternation of decimetre-thick dunitic layers concordant with weakly foliated mantle harzburgites (Fig. 2a, b). The latter are characterized by millimetre- to

centimetre-size rounded to porphyroclastic orthopyroxenes and submillimetric spinels within a matrix of variably serpentinized olivine matrix (average modal composition ol:opx:sp = 79:20:1 vol%; Kelemen et al., 2021a; 2021b). Rare centimetre-thick pyroxenite veins are found within the mantle harzburgites (Fig. 2c, d) and are in places folded by the harzburgite foliation (see Kelemen et al., 2021c). The mantle sequence also displays widespread plagioclase impregnation of the peridotites (dunite and harzburgite), concordant with the weak orthopyroxene foliation of the harzburgites. Additionally, the recovered peridotites are crosscut by discordant millimetre- to centimetre-thick gabbroic dikelets. This study focuses on the spinel-facies evolution recorded by the mantle sequence; detailed characterization of the plagioclase-facies impregnation and intrusion will be provided in a separate contribution. Accordingly, we sampled 6 spinel harzburgites and 1 spinel pyroxenite vein from Hole CM2B (Fig. 1d).

The spinel harzburgites are characterized by a porphyroclastic texture of olivine, orthopyroxene and irregular spinel (Fig. 3a), defining a weak foliation with a shape preferred orientation of orthopyroxene and trails of elongated and corroded spinel. Olivine modal composition ranges up to 85 vol%; olivine is highly serpentinized but kink bands are preserved in some millimetre-size crystals. The centimetre-size pyroxenes observed within the olivine matrix at macroscopic scale (Figs. 2, 3a and b), ranging between 15 and 30 vol%, can occur either as aggregates of sub-millimetric undeformed orthopyroxene, clinopyroxene and spinel neoblasts showing equilibrated textures (Fig. 3c, e), or as large porphyroclastic orthopyroxenes showing clinopyroxene exsolutions (Fig. 3d). Minor primary clinopyroxene, ranging from 100 μm to 200 μm in size and from 1 to 2 vol%, shows cusped resorbed shapes and in places the occurrence of orthopyroxene exsolutions. Olivine often shows lobate contacts with irregular spinels, clinopyroxenes and orthopyroxenes (Fig. 3c, d). Notably, olivine can also be found interstitial to the pyroxene recrystallized aggregates, defining lobate contacts with otherwise equilibrated crystals (Fig. 4).

The spinel pyroxenite is mainly characterized by an aggregate of sub-millimetric undeformed orthopyroxenes and minor clinopyroxenes and spinel showing equilibrated textures (Fig. 3f). Minor irregular and deformed orthopyroxene porphyroclasts can be found within the crystal aggregate. The pyroxenite vein shows a strongly irregular contact with its host spinel harzburgite (Fig. 3b, f), with widespread lobate contacts between the olivine matrix and the pyroxenes. Notably, olivine is also found within the pyroxenite vein, showing interstitial textures and lobate contacts with equilibrated pyroxene crystals commonly showing triple grain junctions (Fig. 3f).

Energy Dispersive Spectrometry (EDS) maps performed in recrystallized orthopyroxene-clinopyroxene-spinel aggregates are a useful tool to document the textural and chemical complexity characterizing the crystal aggregates. Fig. 4 highlights the following features: i) porphyroclastic orthopyroxene shows widespread occurrence of clinopyroxene exsolutions (Fig. 4b, c); ii) the largest recrystallized orthopyroxenes (*opx recryst 1* in the following) showing triple grain junctions are frequently associated with interstitial clinopyroxene and often show the occurrence of clinopyroxene exsolutions (Fig. 4a, b, d); iii) the smallest aggregates of orthopyroxene (*opx recryst 2* in the following) are rarely associated to interstitial clinopyroxene and show no clinopyroxene exsolutions (Fig. 4a, b, c). Fig. 4 also shows the common occurrence of interstitial olivine within the pyroxene aggregates, developing lobate contacts with the equilibrated orthopyroxene crystals.

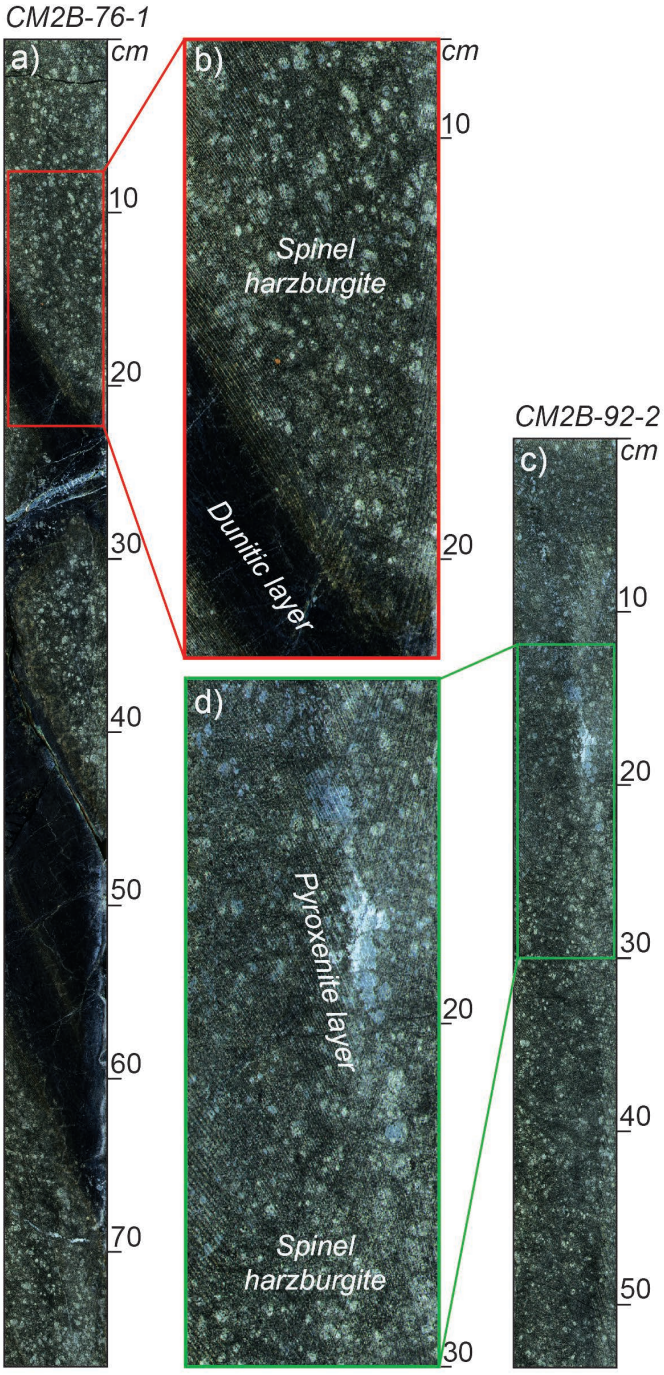

Fig. 2 - Representative petrographic features of the spinel-facies evolution of the Oman ophiolite upper mantle: a) Association between poorly foliated spinel harzburgites and decimetre-thick dunitic layers; b) Close-up of the gradational contact between poorly foliated spinel harzburgites and dunitic layer; c) Association between a pyroxenite vein and its host spinel harzburgite; d) Close-up of the partially dissolved pyroxenite vein.

ANALYTICAL METHODS

Mineral major element Electron Probe Micro-Analyses (EPMA) were performed on 6 samples, including 5 spinel harzburgites and 1 spinel pyroxenite. Major element (SiO_2, TiO_2, Al_2O_3, Cr_2O_3, FeO, MgO, MnO, CaO, NiO, Na_2O and K_2O) compositions of olivine, orthopyroxene, clinopyroxene and spinel were analyzed by JEOL JXA 8200 Superprobe equipped with five wavelength-dispersive (WDS) spectrometers, an energy dispersive (EDS) spectrometer, and a cathodo-

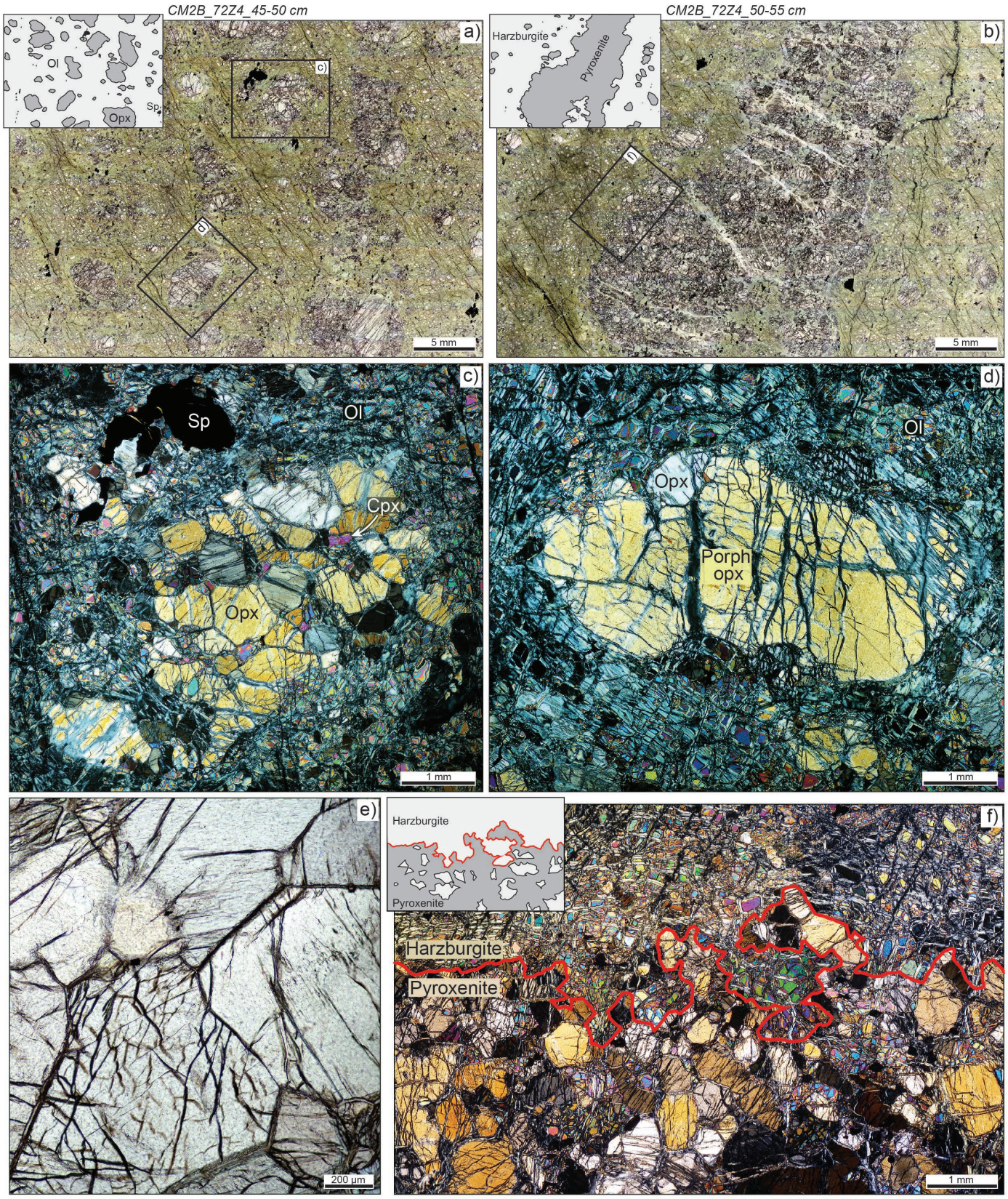

Fig. 3 - Photomicrographs of the representative petrographic features characterizing the Wadi Tayin spinel harzburgite and spinel pyroxenite: a) Spinel harzburgite. Black boxes indicate the location of close-ups c) and d); b) Partially dissolved spinel pyroxenite vein. The black box indicates the location of close-up f); c) Crossed-nicols photomicrograph of partially dissolved spinel crystal and an orthopyroxene aggregate showing lobate contacts with partially serpentinized olivine matrix; d) Crossed-nicols photomicrograph of a porphyroclastic orthopyroxene showing lobate contacts with partially serpentinized olivine matrix; e) Detail of recrystallized orthopyroxene aggregate showing triple grain junctions; f) Crossed-nicols photomicrograph of the contact between the pyroxenite vein and the spinel harzburgite. The dashed red line outlines the irregular contact. The top left insets in a), b) and f) show line drawings evidencing pyroxene crystals within the matrix of partly serpentinized olivine.

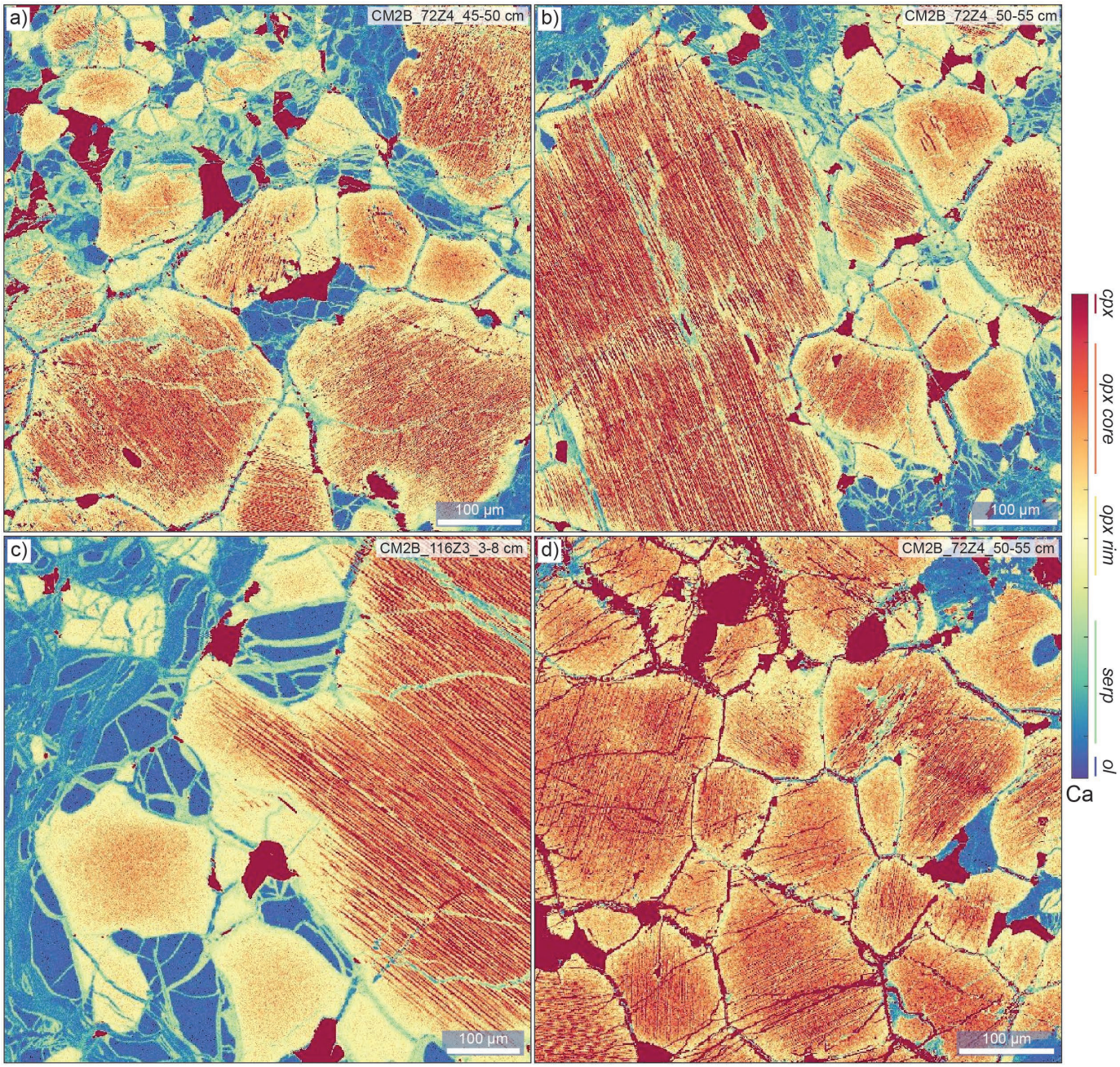

Fig, 4 - EDS chemical maps of Ca within aggregates of partially recrystallized orthopyroxenes. Dark red is clinopyroxene and dark blue is olivine, see colour bar and legend for more detail: a) Harzburgite CM2B_72Z4_45-50cm; b) Harzburgite CM2B_72Z4_50-55cm; c) Harzburgite CM2B_116Z3_3-8cm; d) Pyroxenite CM2B_72Z4_50-55cm.

luminescence detector (accelerating potential 15 kV, beam current 15nA), operating at the Dipartimento di Scienze della Terra, University of Milano. The analyses of all elements were performed with a 30-second counting time. Additionally, EDS maps of Ca were performed within recrystallized orthopyroxene aggregates for petrographic purposes, in order to identify different generations of orthopyroxenes, as well as zones where to perform areal analyses of exsolved minerals. The latter areal analyses (~ 150x150μm) are designed to "reconstruct" the composition of a crystal core prior to exsolution. The stoichiometry of areal analyses has been used as a mean of checking the quality of the primary chemical composition reconstruction. We performed areal analyses of the porphyroclastic orthopyroxenes and of the largest recrystallized orthopyroxenes (*opx recryst 1*), both showing the occurrence of clinopyroxene exsolutions.

MINERAL CHEMISTRY

The major element compositions of the rock-forming minerals, namely olivine, spinel, clinopyroxene and orthopyroxene, are reported in Tables S1-S4 of the Supplementary Material. Mineral compositions within the peridotites and the pyroxenite are similar; this study focuses on mineral compositions in harzburgites.

Olivines (Table S1) are characterized by homogeneous compositions in both spinel harzburgites and pyroxenites, with Mg-numbers (Mg# = 100 x Mg/[Mg + Fe] mol%) ranging from 90.2 mol% to 91.1 mol%, and elevated NiO contents (0.32-0.52 wt%), falling within the compositional field reported for spinel harzburgites from the Wadi Tayin Massif (Hanghøj et al., 2010) and within the compositional

range of residual peridotites worldwide (Warren, 2016).

Spinels (Table S2) analyzed within spinel harzburgites show narrow compositional variations, with elevated Mg-numbers (Mg# = 48.3-59.6 mol%) and Cr-numbers (100 x Cr/[Cr + Al] = 50.2-55.5 mol%) (Fig. 5a). These compositions plot on the most depleted end of the depleted mantle melting trend (Warren, 2016) and correspond to estimated degrees of melting of over 15% following Hellebrand et al. (2002). Additionally, spinels show low TiO_2 contents (Fig. 5b), in agreement with their refractory character and the lack of refertilization veinlets within the analyzed samples (e.g., Hanghøj et al., 2010; Sani et al., 2020). These compositions are consistent with those reported in spinel harzburgites from the Wadi Tayin Massif (Hanghøj et al., 2010) and from highly refractory abyssal peridotites (Dick and Bullen, 1984; Warren, 2016).

Clinopyroxenes (Table S3) analyzed within the spinel harzburgites and pyroxenite have been identified as relics of primary clinopyroxene showing cusped shapes and interstitial within recrystallized and equilibrated crystal aggregates (Figs. 3c and 4). Both clinopyroxene textures show similar compositions, with elevated Mg-numbers (Mg# = 91.4-93.5 mol%), low Al_2O_3 (2.13-3.02 wt%; Fig. 6a), Na_2O (0.07-0.37 wt%; Fig. 6b) and TiO_2 contents (0.01-0.15 wt%; Fig. 6c) with respect to the compositional fields of Oman residual peridotites from the northern (Fizh Massif; Takazawa et al., 2003; Yoshikawa et al., 2015), central (Wadi Sarami; Khedr et al., 2014), and southern ophiolitic massifs (Wadi Tayin; Hanghoj et al., 2010), as well as the compositional fields of Alpine peridotites (Basch et al., 2019; Rampone et al., 2020) and abyssal peridotites worldwide (Warren, 2016). Notably, a negative correlation is usually observed between Mg-numbers and Al_2O_3 contents of clinopyroxenes from residual peridotites, together with a positive correlation between Na_2O, Al_2O_3 and TiO_2 (e.g., Warren, 2016; Basch et al., 2019). Such correlations are not observed in our Oman peridotite samples, which plot at the depleted end of the composition field of abyssal peridotites (e.g., Takazawa et al., 2003; Yoshikawa et al., 2015), and show no differences in composition between the primary relic clinopyroxenes and the secondary clinopyroxene in the recrystallized aggregates.

Orthopyroxenes (Table S4) analyzed within the spinel harzburgites and pyroxenite have been identified as orthopyroxene porphyroclasts (Fig. 3d) and as two different generations of recrystallized orthopyroxene presenting triple grain junctions within crystal aggregates (Figs. 3c, e and 4). All orthopyroxenes show elevated Mg-numbers (Mg# = 90.6-91.6 mol%), low Al_2O_3 (1.72-2.30 wt%; Fig. 7a) and Cr_2O_3 contents (0.58-0.81 wt%; Fig. 7b) with respect to the compositional fields of Oman residual peridotites from the northern (Fizh Massif; Takazawa et al., 2003; Yoshikawa et al., 2015) and central ophiolitic massifs (Wadi Sarami; Khedr et al., 2014), as well as the compositional field of abyssal peridotites worldwide (Warren, 2016), but plot within the compositional range previously reported within the southern Oman ophiolites (Wadi Tayin; Hanghøj et al., 2010). Except for slightly higher average Mg-numbers and lower Al_2O_3 and Cr_2O_3 contents (Fig. 7) in the smallest recrystallized orthopyroxene aggregates (*opx recryst 2*), no substantial compositional differences are observed between the punctual analyses of orthopyroxene porphyroclasts and the two generations of recrystallized orthopyroxenes. Such homogeneous compositions could result from the last recrystallization process leading to the formation of the clinopyroxene exsolutions within orthopyroxene porphyroclasts and the largest recrystallized orthopyroxenes. To assess the chemical composition of the latter crystals prior to exsolution, we performed areal analyses of the exsolved crystals, which revealed decreasing Ca contents (Fig. 7c) from orthopyroxene porphyroclasts (CaO_{opx1} = 2.02-2.99 wt%) to the first ($CaO_{recryst1}$ = 2.26-2.77 wt%) and second generation ($CaO_{recryst2}$ = 1.20-1.89 wt%) of recrystallized orthopyroxene aggregates.

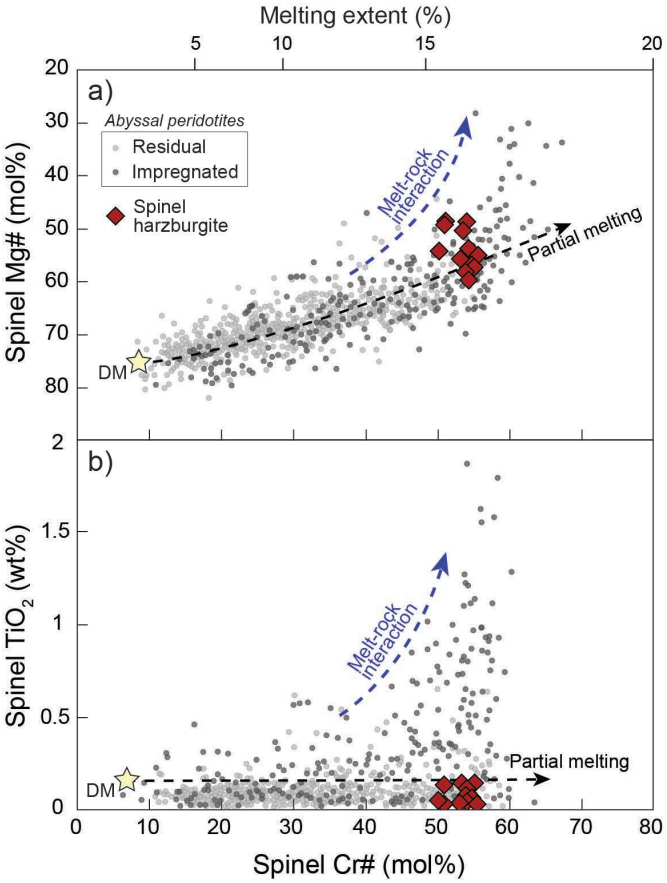

Fig. 5 - Spinel major elements chemistry; a) Cr-number vs Mg-number; b) Cr-number vs TiO_2 of partially resorbed spinels analysed in the Wadi Tayin spinel harzburgite and pyroxenite. Also shown are compositions of spinels from residual and impregnated abyssal peridotites, after Warren (2016) and Sani et al. (2020) and DM compositions after Salters and Stracke (2004). Partial melting and melt-rock interaction trends are after Sani et al. (2020) and estimated degree of melting extent is based on the Cr-number, following Hellebrand et al. (2002).

GEOTHERMOMETRIC ESTIMATES

To provide constraints on the thermal state of the Oman residual spinel harzburgites, we computed geothermometric estimates of the primary assemblage and the subsequent recrystallization events. Given that the primary assemblage and recrystallized aggregates are formed of orthopyroxene-clinopyroxene-spinel crystals, we report the temperature estimates of three independent and widely used geothermometers, namely 1) orthopyroxene-clinopyroxene from Taylor (1998), 2) orthopyroxene-clinopyroxene from Brey and Köhler (1990) and 3) single clinopyroxene from Nimis and

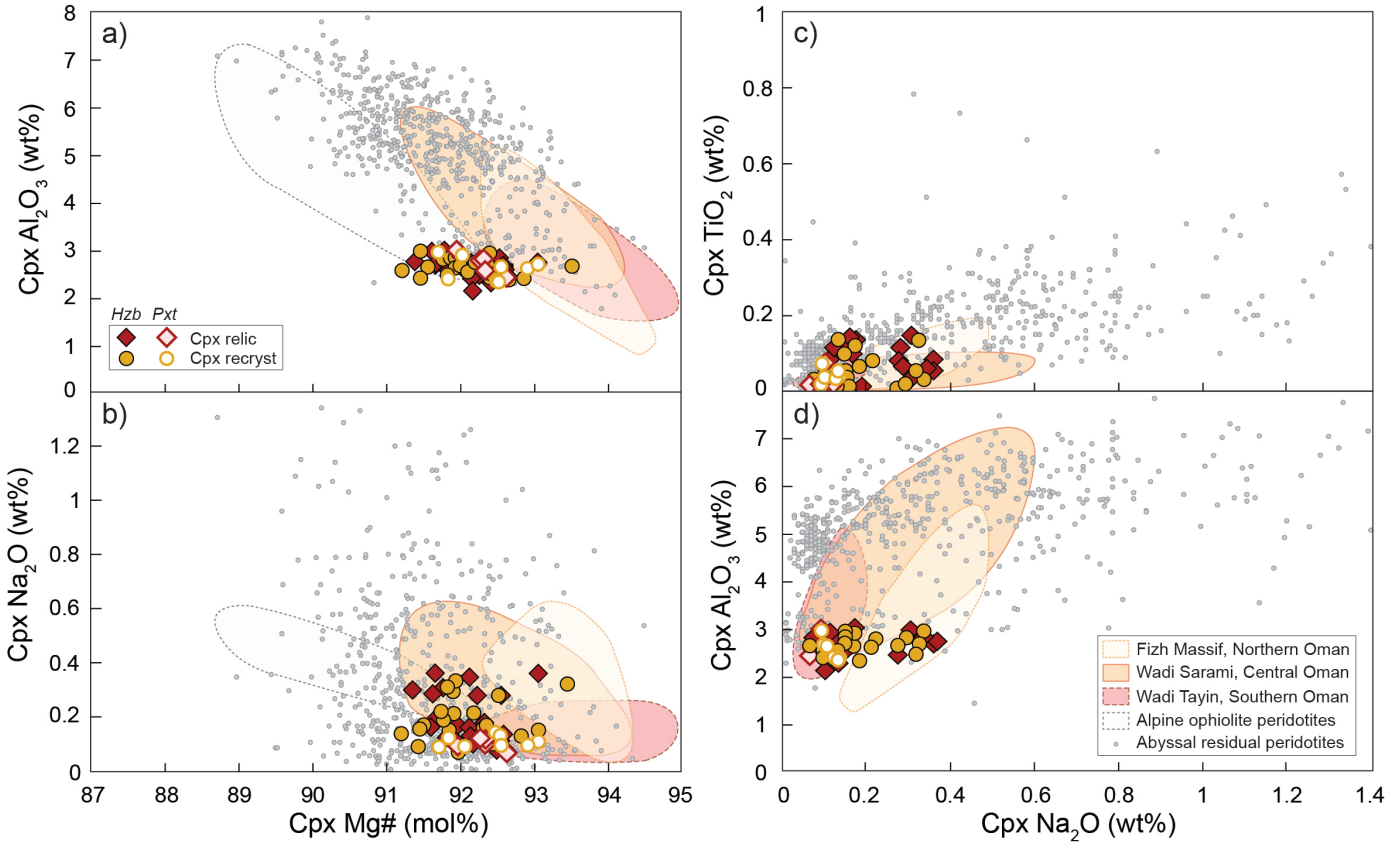

Fig. 6 - Clinopyroxene major elements chemistry from spinel harzburgites (Hzb) and spinel pyroxenite (Pxt): a) Mg-number vs Al_2O_3; b) Mg-number vs Na_2O; c) Na_2O vs TiO_2; d) Na_2O vs Al_2O_3 of relic and granoblastic clinopyroxenes analysed in the Wadi Tayin mantle section. Also shown are compositional fields of clinopyroxenes analysed in peridotites from the Fizh Massif (Takazawa et al., 2003; Yoshikawa et al., 2015), Wadi Sarami (Khedr et al., 2014) and Wadi Tayin (Hanghøj et al., 2010) in the Oman ophiolite, from Alpine ophiolites (Basch et al., 2019; Rampone et al., 2020) and abyssal peridotites (Warren, 2016; Sani et al., 2020).

Taylor (2000). The equilibrium temperature estimates are representative of: (1) equilibrium temperature prior to partial recrystallization stage, using couples of areal and punctual analyses of orthopyroxene and clinopyroxene porphyroclasts, within both harzburgites and pyroxenite (*Opx1-Cpx1* in Fig. 8); (2) Recrystallization temperature of the equilibrated crystal aggregates, using couples of areal and punctual analyses of recrystallized orthopyroxenes and clinopyroxenes within both harzburgites and pyroxenites (*Opx2-Cpx2* in Fig. 8). Overall, the three geothermometers used yield similar results (Table S5) and are presented as a single range.

The areal analyses of the porphyroclastic assemblage (dark red symbols in Fig. 8) yield slightly higher temperature estimates within the spinel harzburgite, in the range of 996-1104°C (average of 1057°C), respect to the spinel pyroxenite, in the range of 962-1044°C (average of 997°C). The areal analyses of the recrystallized assemblage (orange symbols in Fig. 8) give similar estimated temperatures within the spinel harzburgites and pyroxenites, in the range of 908-1036°C (average of 986°C) and 955-1015°C (average of 983°C), respectively. Punctual analyses of the porphyroclastic assemblage (light red symbols in Fig. 8) yield similar results within the spinel harzburgites and pyroxenite, in the range 862-1000°C (average of 933°C) and 888-1044°C (average of 949°C), respectively. Similarly, punctual analyses of the recrystallized assemblage (yellow symbols in Fig. 8) estimate similar temperatures within the spinel harzburgites and pyroxenite, in the range 837-1031°C (average of 929°C) and 820-1015°C (average of 919°C), respectively.

The higher temperature estimates obtained for areal analyses testify of the efficiency of the reconstruction of the crystal composition prior to secondary exsolution and further re-equilibration. Conversely, all punctual analyses yield similar equilibrium temperatures (Table S5), as a result of a global "reset" of the compositions at lower temperatures during the last registered cooling event, i.e., the exsolution stage. Our geothermometric estimates therefore document a progressive cooling of this mantle domain from equilibrated porphyroclasts (~ 1000-1050°C) to the recrystallization event leading to the formation of the crystal aggregates (~ 950-1000°C) and finally the exsolution of both orthopyroxene porphyroclasts and equilibrated aggregates (~ 900-950°C).

DISCUSSION

Chronology of the magmatic and subsolidus evolution

The Wadi Tayin upper mantle peridotites are commonly documented as showing "*coarse-grained porphyroclastic textures associated with asthenospheric mantle flow*" (Godard et al., 2000), or "*typical characteristic porphyroclastic mantle textures*" (Kelemen et al., 2021a; 2021b). Consistently, our harzburgite samples from CM1A and CM2B exhibit a weak foliation defined by an orthopyroxene shape-preferred orientation at macroscopic scale (Fig. 2a, b). However, these centimetre-size elongated orthopyroxene "porphyroclasts" mostly occur as recrystallized aggregates of equilibrated orthopyroxenes, clinopyroxenes and spinel (Figs. 3c, e and

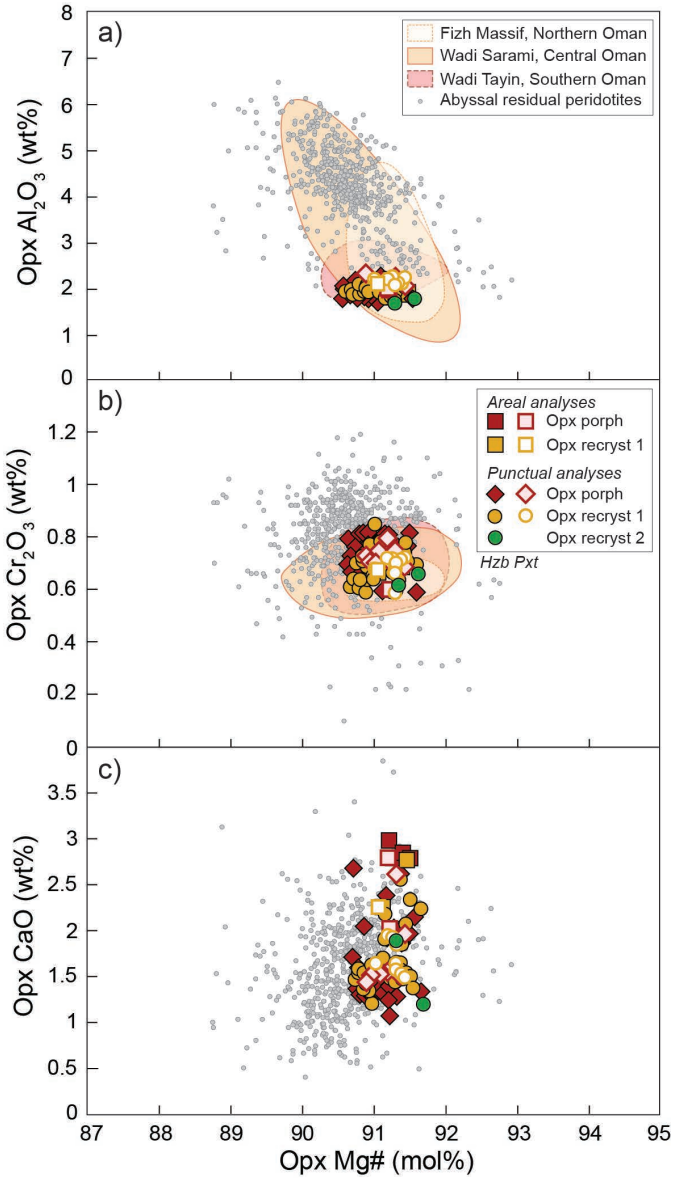

Fig. 7 - Orthopyroxene major elements chemistry from spinel harzburgites (Hzb) and spinel pyroxenite (Pxt): a) Mg-number vs Al_2O_3; b) Mg-number vs Cr_2O_3; c) Mg-number vs CaO of porphyroclastic and recrystallized orthopyroxenes analysed in the Wadi Tayin mantle section. Also shown are compositional fields of orthopyroxenes analysed in peridotites from the Fizh Massif (Takazawa et al., 2003; Yoshikawa et al., 2015), Wadi Sarami (Khedr et al., 2014) and Wadi Tayin (Hanghøj et al., 2010) in the Oman ophiolite, and from abyssal peridotites worldwide (Warren, 2016; Sani et al., 2020).

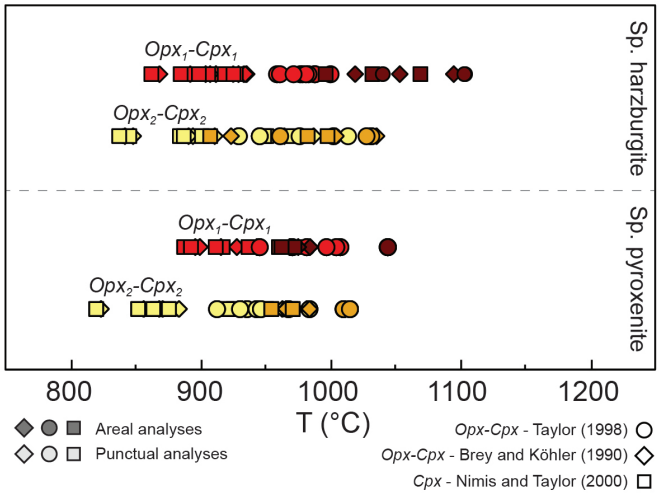

Fig. 8 - Geothermometric estimates of the equilibration temperature of clinopyroxene-orthopyroxene couples after Brey and Köhler (1990) and Taylor (1998), and single clinopyroxene after Nimis and Taylor (2000). Red-tone colours refer to the primary opx_1-cpx_1 paragenesis and yellow-tone colours refer to the recrystallized opx_2-cpx_2 paragenesis. Darker colours represent geothermometric estimated obtained from areal analyses, whereas light colours are obtained from punctual analyses.

4). Two generations of orthopyroxene neoblasts can be identified within the crystal aggregates, with the occurrence of clinopyroxene exsolutions within the largest recrystallized orthopyroxenes (Fig. 4) and a progressive decrease in Ca contents from larger to smaller crystals (Fig. 7c). Such extensive subgrain formation and recrystallization of primary orthopyroxene porphyroclasts evidence progressive cooling of this mantle portion within the lithospheric mantle (Borghini et al., 2010; 2011; Basch et al., 2020), as confirmed by our geothermometric estimates (Fig. 8). Similar partial recrystallization is observed within the spinel pyroxenite vein (Figs. 3f and 4), suggesting that the association between spinel harzburgites and pyroxenites predates this cooling event (Fig. 9a, b).

Additionally, interstitial olivine commonly develops lobate contacts on the rims and within the recrystallized pyroxene aggregates (Figs 3c, d, and 4), and at the contact between the pyroxenite vein and the spinel harzburgite (Fig. 3f). This textural feature indicates partial dissolution of pyroxenes and crystallization of interstitial olivine and has been commonly described in ophiolites and abyssal peridotites worldwide (e.g., Kelemen et al., 1995a; Dick et al., 2010; Laukert et al., 2014; Dygert et al., 2016; Warren, 2016; Basch et al., 2019; Rampone et al., 2020). It is associated with a reactive porous flow process resulting from the expansion of the stability field of olivine during the upward percolation of a tholeiitic melt in a mantle column (e.g., Kelemen et al., 1995b; Liang, 2003; Morgan and Liang, 2005). This process, occurring at spinel-facies depths, progressively dissolves mantle pyroxenes and crystallizes secondary olivine and can ultimately lead to the formation of replacive dunites (e.g., Kelemen et al., 1995a; 1995b; Morgan and Liang, 2005). Remarkably, the interstitial olivine is found within the recrystallized pyroxene aggregates and partially dissolves the equilibrated crystals displaying triple junctions (Figs. 4 and 9c). This places an important temporal constraint on the reactive porous flow process, which likely occurred after the cooling and associated recrystallization process. Our geothermometric estimates indicate that the Oman uppermost mantle cooled substantially, to temperatures of ~ 950-1000°C down to spinel-facies depths (P > ~ 7 kbar; Fumagalli et al., 2017). Based on textural observations, we here infer that cooling at lithospheric conditions took place before the reactive porous flow process, in turn indicating that diffuse reactive percolation of olivine-saturated melts occurred at spinel facies within a previously cooled and partially recrystallized harzburgite-pyroxenite association (Fig. 9c). This is consistent with the results of geochemical investigations on the main harzburgitic mantle section by Godard et al. (2000), suggesting that the Oman harzburgites were pervasively affected by diffuse melt flow at shallow levels, leading to olivine addition.

In the succession of processes that we here propose, the spinel-facies pyroxenite vein is primarily associated with mantle harzburgites and could represent either: i) metamor-

phic recycling of subducted oceanic crust (e.g., Allègre and Turcotte, 1986; Morishita and Arai, 2001; Morishita et al., 2003; Yu et al., 2010), ii) "refertilization" of a depleted mantle during reactive melt percolation (e.g., Garrido and Bodinier, 1999; van Acken et al., 2010; Laukert et al., 2014; Borghini et al., 2016) or, iii) spinel-facies segregations from a pyroxene-saturated melt (e.g., Takazawa et al., 1999; Dantas et al., 2007; Gysi et al. 2011; Basch et al., 2019). The pyroxenes and spinels forming the harzburgites and pyroxenites show similar major element compositions that do not allow a detailed assessment of the pyroxenite veins formation process. However, we emphasize that the pyroxenite is primarily associated with strongly depleted spinel harzburgites showing only relics of clinopyroxenes and recording high degrees of melting (> 15%; Fig. 5a, b; e.g., Godard et al., 2000; Le Mée et al., 2004). We infer that a pyroxenite vein would not have been preserved during such extensive melting (e.g., Stracke et al., 2000), and we therefore favour a process during which the pyroxenite formed within the extending lithosphere, during refertilization or segregation from melts percolating within the upwelling mantle, as it was previously documented in the Maqsad and Mansah area of the Oman ophiolite (e.g., Nicolle et al., 2016). Notably, the elevated orthopyroxene modal content characterizing the pyroxenite vein (Figs. 3f, and 4d) could possibly indicate a reactive component of its parental melt, that partially dissolved orthopyroxene from the percolated harzburgites and increased its orthopyroxene saturation prior to crystallization (e.g., Borghini et al., 2016; Basch et al., 2019).

To summarize, the studied peridotites and associated pyroxenite from the Wadi Tayin uppermost mantle record the magmatic formation of spinel-facies pyroxenite veins (Fig. 9a), followed by cooling and partial recrystallization of orthopyroxene porphyroclasts and pyroxenite veins (Fig. 9b), and reactive porous flow at spinel facies (Fig. 9c).

Implications on the geodynamic evolution of the Oman ophiolite

Although the geodynamic setting in which the Oman oceanic lithosphere formed and evolved is still debated, accumulating structural and chemical evidence progressively drove a conceptual shift in the envisioned formation environment of the Oman lithosphere, from mid-ocean ridge (e.g., Nicolas et al., 2000; Godard et al., 2003) to a subduction-related proto-arc setting (e.g., MacLeod et al., 2013; Goodenough et al., 2014; Belgrano and Diamond, 2019). In this debate, extensive field mapping of the large-scale mantle and intrusion structures are crucial in defining the evolution of this complex system (e.g., Ceuleneer et al., 1996; Python and Ceuleneer, 2003). Yet, we argue that a detailed petrographic description of the different processes recorded by the mantle lithologies is equally important in defining the evolution of the oceanic lithosphere. In this study, we document the cooling and partial recrystallization of the mantle at lithospheric conditions, prior to the magmatic history recorded within CM1A and CM2B drillcores. The latter magmatic history includes the reactive melt percolation of olivine-saturated melts, the impregnation of the mantle section at plagioclase facies and the formation of crosscutting gabbroic dikelets and anorthosite and diopsidite veinlets (Kelemen et al., 2021a; 202b). Although the present study focuses on the spinel-facies evolution of this mantle portion, further petrographic and geochemical studies of the plagioclase-facies magmatic events will be carried out in a complementary study, allowing detailed constrain of the magmatic affinity of this subsequent magmatism.

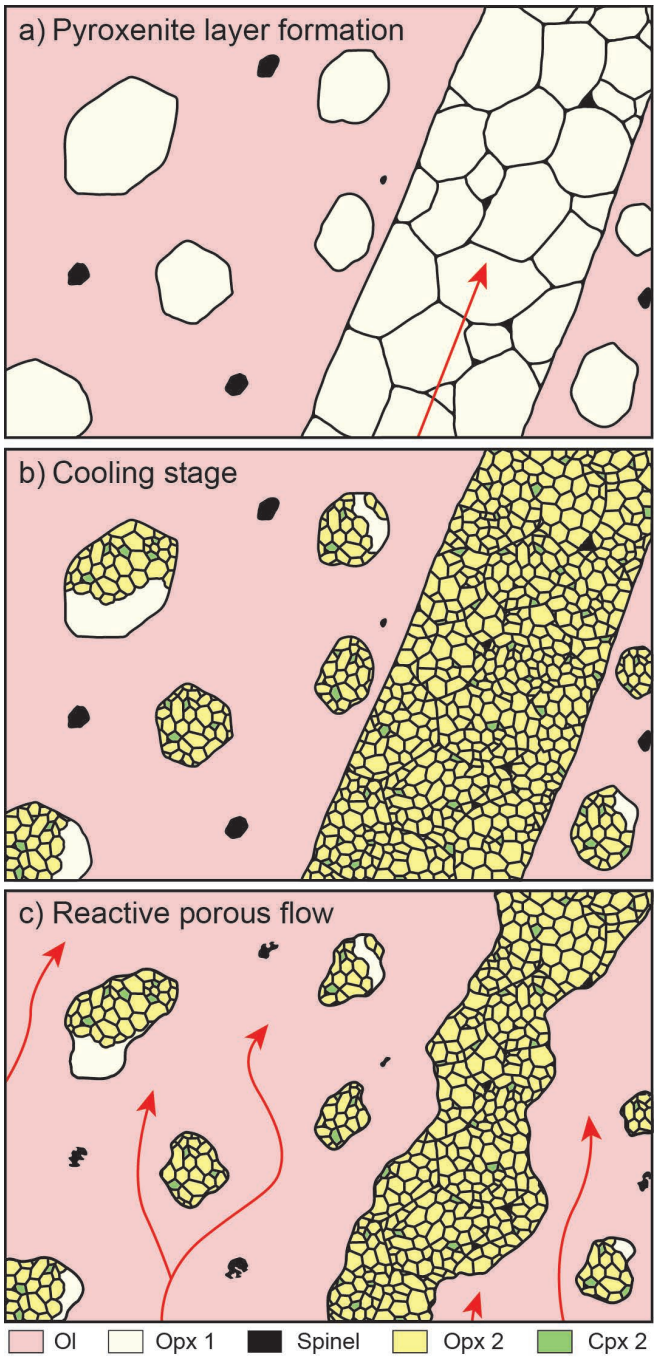

Fig. 9 - Interpretative sketch retracing the spinel-facies evolution steps documented in the Wadi Tayin peridotites and pyroxenite: a) formation of pyroxenite veins during whether high-pressure melt segregation or melt-peridotite interaction; b) accretion of the Wadi Tayin mantle at lithospheric levels during progressive cooling of the upper mantle; c) reactive porous flow, leading to partial dissolution of peridotite and pyroxenite pyroxenes and crystallization/growth of interstitial olivine.

In a first attempt to replacing the documented spinel-facies evolution in the context of formation of the Oman oceanic lithosphere, it is crucial to constrain the geodynamic setting in which the mantle section was able to cool substantially down to spinel facies depths. Given that the accretion of the Oman ophiolite occurred at a fast-spreading ridge (e.g., Rioux et al., 2013), constant melt addition at the ridge axis most likely led to a buffer of the isotherms in the vicinity of the spreading centre. Thus, if the Oman lithosphere formed at a mid-ocean ridge, its cooling would only have been possible away from the ridge

axis. Consequently, all the documented magmatic episodes following the cooling event would not be related to the main accretion phase but rather to a minor "off-axis" magmatic phase, similar to what is documented by Nicolle et al. (2016) for the Mansah diapir. In alternative, the formation of the Oman lithosphere above a nascent subduction would involve a previously cooled, depleted mantle section, during reactivation of a pre-existing oceanic lithosphere as previously suggested by Godard et al. (2000) and Python and Ceuleneer (2003). In this scenario, the magmatic events following the cooling of the upper mantle could belong to the accretionary phase of the Oman lithosphere in a proto-arc setting, as it is increasingly suggested by recent studies of the Oman ophiolite (e.g., MacLeod et al., 2013; Goodenough et al., 2014; Belgrano and Diamond, 2019; Guilmette et al., 2021). Together with this study, detailed petrographic and geochemical investigations of the mantle impregnation features and crosscutting dikes are needed and will provide accurate constraints on the formation environment of the Oman lithosphere sampled at sites CM1A and CM2B.

CONCLUDING REMARKS

This study provides a petrographic and chemical investigation of the upper mantle section sampled at OmanDP CM sites, aimed at constraining the spinel-facies evolution recorded in the residual harzburgites and associated pyroxenites. The main processes that we document are: i) formation of pyroxenite veins as melt segregations, ii) cooling of the upper mantle and partial re-equilibration of the mantle harzburgites and pyroxenites and, iii) reactive porous flow and partial dissolution of mantle pyroxenes. Most importantly, this chronological evolution involves cooling at lithospheric conditions prior to reactive melt porous flow, plagioclase-facies mantle impregnation and formation of gabbroic dikelets. Further geochemical studies of the plagioclase-facies magmatism will allow to thoroughly assess if the latter is correlated with the main accretionary phase of the Oman crust or with a late off-axis magmatism in an open-ocean setting, thus providing substantial constraints on the geodynamic environment of formation of the Oman lithosphere.

ACKNOWLEDGEMENTS

We thank Giulio Borghini for his work as editor, as well as two anonymous reviewers that provided crucial insights that improved the quality of the manuscript. Martina Raveni is acknowledged for her preliminary investigations on CM cores during the bachelor thesis. We thank Paolo Campanella and Alessandra Gavoglio for realization of the thin section, as well as Andrea Risplendente for assistance with the EPMA and Laura Negretti for assistance with the areal analyses. This research has been supported by the Italian Ministry of University and Research (MUR) through the grant [ECORD-IODP Italia 2021] attributed to Valentin Basch, and the grant [PRIN-2015C5LN35] "Melt-rock reaction and melt migration in the MORB mantle through combined natural and experimental studies". This research used samples provided by the Oman Drilling Project (OmanDP). The OmanDP were funded from the International Continental Scientific Drilling Project (Kelemen, Matter, Teagle Lead PIs), the Sloan Foundation-Deep Carbon Observatory (Grant 2014-3-01, Kelemen PI), the National Science Foundation (NSF-EAR-1516300, Kelemen lead PI), NASA-Astrobiology Institute (NNA15BB02A, Templeton PI), the German Research Foundation (DFG: KO 1723/21-1, Koepke PI), the Japanese Society for the Promotion of Science (JSPS no:16H06347, Michibayashi PI; and KAKENHI 16H02742, Takazawa PI), the European Research Council (Adv: no.669972; Jamveit PI), the Swiss National Science Foundation (SNF:20FI21_163,073, Früh-Green PI), JAMSTEC, the TAMU-JR Science Operator, and contributions from the Sultanate of Oman Ministry of Regional Municipalities and Water Resources, the Oman Public Authority of Mining, Sultan Qaboos University, CRNS-Univ. Montpellier II, Columbia University of New York, and the University of Southampton.

REFERENCES

Abily B. and Ceuleneer G., 2013. The dunitic mantle-crust transition zone in the Oman ophiolite: residue of melt-rock interaction, cumulates from high-MgO melts, or both? Geology: 41: 67-70, doi: 10.1130/G33351.1.

Akizawa N., Ozawa K., Tamura A., Michibayashi K. and Arai S., 2016. Three-dimensional evolution of melting, heat and melt transfer in ascending mantle beneath a fast-spreading ridge segment constrained by trace elements in clinopyroxene from concordant dunites and host harzburgites of the Oman Ophiolite. J. Petrol., 57: 777-814, doi: 10.1093/petrology/egw020.

Alabaster T., Pearce J.A. and Malpas J., 1982. The volcanic stratigraphy and petrogenesis of the Oman ophiolite complex, Contrib. Miner. Petrol., 81: 168-183.

Allègre C.J. and Turcotte D.L., 1986. Implications of a two-component marble-cake mantle. Nature, 323: 123-127.

Anonymous, 1972. Penrose field conference on ophiolites. Geotimes, 17: 24-25.

Basch V., Borghini G., Fumagalli P., Rampone E., Gandolfo A. and Ferrando C., 2020. Plagioclase-facies thermobarometric evolution of the External Liguride pyroxenite-bearing mantle (Suvero, Italy). Ofioliti, 45: 1-12, doi: 10.4454/Ofioliti.v45il.529.

Basch V., Rampone E., Borghini G., Ferrando C. and Zanetti A., 2019. Origin of pyroxenites in the oceanic mantle and their implications on the reactive percolation of depleted melts. Contrib. Miner. Petrol., 174, 97, doi: 10.1007/s00410-019-1640-0.

Belgrano T.M. and Diamond L.W., 2019. Subduction-zone contributions to axial volcanism in the Oman-U.A.E. ophiolite. Lithosphere, 11: 399-411, doi: 10.1130/L1045.1.

Belgrano T.M., Diamond L.W., Vogt Y., Biedermann A.R., Gilgen S.A. and Al-Tobi K., 2019. A revised map of volcanic units in the Oman ophiolite: insights into the architecture of an oceanic proto-arc volcanic sequence. Solid Earth, 10: 1181-1217, doi: 10.5194/se-10-1181-2019.

Benoit M., Ceuleneer G. and Polvé M., 1999. The remelting of hydrothermally altered peridotite at mid-ocean ridges by intruding mantle diapirs. Nature, 402: 514-518.

Beurrier, M., 1987. Géologie de la Nappe Ophiolitique de Samail dans les Parties Orientale et Centrale des Montagnes d'Oman. PhD thesis. 128. Université Pierre et Marie Curie, Paris 6. Doc. BRGM Orléans, pp. 1–412.

Beurrier M., Ohnenstetter M., Cabanis B., Lescuyer J.L., Tegyey M. and Le Metour J., 1989. Géochimie des filons doléritiques et des roches volcaniques ophiolitiques de la nappe de Semail; contraintes sur leur origine géotectonique au Crétacé supérieur. Bull. Soc. *Géol*. Fr., V(2): 205-219, doi: 10.2113/gssgfbull.V.2.205.

Borghini G., Fumagalli P. and Rampone E., 2010. The stability of plagioclase in the upper mantle: subsolidus experiments on fertile and depleted lherzolite. J. Petrol., 51: 229-254, doi: 10.1093/petrology/egp079.

Borghini G., Fumagalli P. and Rampone E., 2011. The geobarometric significance of plagioclase in mantle peridotites: A link between nature and experiments. Lithos, 126: 42-53, doi:10.1016/j.lithos.2011.05.012.

Borghini G., Rampone E., Zanetti A., Class C., Cipriani A., Hof-

mann A.W. and Goldstein S.L., 2016. Pyroxenite layers in the Northern Apennines' Upper Mantle (Italy)-generation by pyroxenite melting and melt infiltration. J. Petrol., 57:625-653

Boudier F. and Nicolas A., 1985. Harzburgite and lherzolite subtypes in ophiolitic and oceanic environments. Earth and Planet. Sci. Lett., 76: 84-92.

Boudier F. and Nicolas A., 1995. Nature of the Moho Transition Zone in the Oman Ophiolite. J. Petrol., 36: 777-796.

Boudier F., Ceuleneer G. and Nicolas A., 1988. Shear zones, thrusts and related magmatism in the Oman ophiolite: initiation of thrusting on an oceanic ridge. Tectonophysics, 151: 275-296.

Boudier F., Nicolas A., Ildefonse B. and Jousselin D., 1997. EPR microplates, a model for the Oman ophiolite. Terra Nova, 9: 79-82.

Brey G.P. and Köhler T., 1990. Geothermobarometry in four phase lherzolites II. New thermobarometers, and practical assessment of existing thermobarometers. J. Petrol., 31: 1353-1378.

Ceuleneer G., 1991. Evidence for a paleo-spreading center in the Oman ophiolite: Mantle structures in the Maqsad area. In: T. Peters, A. Nicolas and R.G. Coleman (Eds.), Ophiolite genesis and evolution of the oceanic lithosphere, , Kluwer Acad. Norwell, p. 147-173.

Ceuleneer G. and Rabinowicz M., 1992. Mantle flow and melt migration beneath oceanic ridges: Models derived from observation in ophiolites, in mantle flow and melt generation at mid-ocean ridges. In: J.P. Morgan, D.B. Blackman and J.M. Sinton (Eds.), Geophys. Monogr. Ser., 71:123-154, AGU

Ceuleneer G., Monnereau M. and Amri I., 1996. Thermal structure of a fossil mantle diapir inferred from the distribution of mafic cumulates. Nature, 379: 149-153.

Ceuleneer G., Nicolas A. and Boudier F., 1988. Mantle flow patterns at an oceanic spreading center: the Oman peridotites record. Tectonophysics, 151: 1-26.

Dantas C., Ceuleneer G., Gregoire M., Python M., Freydier R., Warren J.M. and Dick H.J.B., 2007. Pyroxenites from the Southwest Indian Ridge, 9°-16°E: cumulates from incremental melt fraction produced at the top of a cold melting regime. J. Petrol., 48: 647-660.

Dick H.J.B. and Bullen T., 1984. Chromian spinel as a petrogenetic indicator in abyssal and alpine-type peridotites and spatially associated lavas. Contrib. Miner. Petrol., 86: 54-76.

Dick H.J.B., Lissenberg C.J. and Warren J.M., 2010. Mantle melting melt transport, and delivery beneath a slow-spreading ridge: the paleo-MAR from 23°15'N to 23°45'N. J. Petrol., 51: 425-467, doi: 10.1093/petro logy/egp088.

Dygert N., Liang Y. and Kelemen P.B., 2016. Formation of plagioclase lherzolite and associated dunite-harzburgite-lherzolite sequences by multiple episodes of melt percolation and melt-rock reaction: an example from the Trinity Ophiolite, California, USA. J. Petrol., 57: 815-838, doi: 10.1093/j.petrology/egw018.

Einaudi F., Godard M., Pezard P., Cochemé J.J., Coulon C., Brewer T. and Harvey P., 2003. Magmatic cycles and formation of the upper oceanic crust at spreading centres: Geochemical study of a continuous extrusive section in the Oman ophiolite. Geochem. Geophys. Geosyst., 4, doi: 10.1029/2002GC000362.

Einaudi F., Pézard P., Cochemé J.J., Coulon C., Laverne C. and Godard, M., 2000. Petrography, geochemistry and physical properties of a continuous extrusive section from the Hilti Massif, Oman ophiolite. Mar. Geophys. Res., 21: 387-407.

Ernewein M., Pflumio C. and Whitechurch H., 1988. The death of an accretion zone as evidenced by the magmatic history of the Sumail ophiolite (Oman), Tectonophysics, 151: 247-274.

Fumagalli P., Borghini G., Rampone E. and Poli S., 2017. Experimental calibration of Forsterite-Anorthite-Ca-Tschermak-Enstatite (FACE) geobarometer for mantle peridotites. Contrib. Miner. Petrol., 172: 38, doi: 10.1007/s00410-017-1352-2.

Garrido C.J. and Bodinier J.L., 1999. Diversity of mafic rocks in the Ronda peridotite: evidence for pervasive melt-rock reaction during heating of subcontinental lithosphere by upwelling asthenosphere. J. Petrol., 40: 729-754.

Godard M., Dautria J.M. and Perrin M., 2003. Geochemical variability of the Oman ophiolite lavas: relationship with spatial distribution and paleomagnetic directions. Geochem. Geophys. Geosyst., 4, doi: 10.1029/2002GC000452.

Godard M., Jousselin D. and Bodinier J.L., 2000. Relationships between geochemistry and structure beneath a palaeo-spreading centre: a study of the mantle section in the Oman ophiolite. Earth Planet. Sci. Lett., 180: 133-148.

Goodenough K.M., Thomas R.J., Styles M.T., Schofield D.I. and MacLeod C.J., 2014. Records of ocean growth and destruction in the Oman-UAE Ophiolite. Elements, 10: 109-114, doi: 10.2113/gselements.10.2.109.

Guilmette C., Smit M.A., van Hinsbergen D.J.J., Gürer D., Corfu F., Charette B., Maffione M., Rabeau O. and Savard D., 2021. Forced subduction initiation recorded in the sole and crust of the Semail Ophiolite of Oman. Nature Geosci., 11: 688-695, doi: 10.1038/s41561-018-0209-2.

Gysi A.P., Jagoutz O., Schmidt M.W. and Targuisti K., 2011. Petrogenesis of pyroxenites and melt infiltrations in the ultramafic complex of Beni Bousera, Northern Morocco. J. Petrol., 52: 1676-1735.

Hacker B.R., Mosenfelder J.L. and Gnos E., 1996. Rapid emplacement of the Oman Ophiolite; thermal and geochronologic constraints. Tectonics, 15: 1230-1247.

Hanghøj K., Kelemen P.B., Hassler D. and Godard M., 2010. Composition and genesis of depleted mantle peridotites from the Wadi Tayin Massif, Oman Ophiolite; major and trace element geochemistry, and Os isotope and PGE systematics. J. Petrol., 51: 201-227, doi: 10.1093/petrology/egp077.

Hellebrand E., Snow J.E. and Mühe R., 2002. Mantle melting beneath Gakkel Ridge (Arctic Ocean): abyssal peridotite spinel compositions. Chem. Geol., 182: 227-235.

Higgie K. and Tommasi A., 2012. Feedbacks between deformation and melt distribution in the crust-mantle transition zone of the Oman ophiolite. Earth Planet. Sci. Lett., 359-360: 61-72, doi: 10.1016/j.epsl.2012.10.003.

Ildefonse B., Billiau S. and Nicolas A., 1995. A detailed study of mantle flow away from diapirs in the Oman ophiolite. In: R.L.M. Vissers and A. Nicolas (Eds.), Mantle and lower crust exposed in oceanic ridges and in ophiolites, p. 163-177, Kluwer, Norwell, Mass.

Ildefonse B., Nicolas A. and Boudier F., 1993. Evidence from the Oman ophiolite for active mantle upwelling beneath a fast-spreading ridge. Nature, 370: 51-53.

Jousselin D., Mainprice D., 1998. Melt topology and seismic anisotropy in mantle peridotites of the Oman ophiolite. Earth Planet. Sci. Lett., 164: 553-568.

Jousselin D. and Nicolas A., 2000. The Moho transition zone in the Oman ophiolite, relation with wehrlites in the crust and dunites in the mantle. Mar. Geophys. Res., 21: 229-241.

Kelemen P.B., Hitehead J.A., Aharonov E. and Jordahl K.A., 1995b. Experiments on flow focusing in soluble porous media, with applications to melt extraction from the mantle. J. Geophys. Res. Solid Earth, 100: 475-496.

Kelemen P.B., Matter J.M., Teagle D.A.H., Coggon J.A. and Oman D.P. Sci. Team, 2021a. Site CM1: Layered gabbros, crustal ultramafic rocks, and mantle harzburgite. In: P.B. Kelemen, J.M. Matter, D.A.H. Teagle, J.A. Coggon et al. (Eds.), Proceed. Oman D.P.. (International Ocean Discovery Program), doi: 10.14379/OmanDP.proc.2020.

Kelemen P.B., Matter J.M., Teagle D.A.H., Coggon J.A. and Oman D.P. Sci. Team, 2021b. Site CM2: Crust-mantle transition zone and into upper mantle. In: P.B. Kelemen, J.M. Matter, D.A.H. Teagle, J.A. Coggon et al. (Eds.), Proceed. Oman D.P.: (International Ocean Discovery Program), doi: 10.14379/OmanDP.proc.2020.

Kelemen, P.B., Matter, J.M., Teagle, D.A.H., Coggon, J.A. and Oman D.P. Sci. Team, 2021c. Site BA1. In: P.B. Kelemen, J.M. Matter, D.A.H. Teagle, J.A. Coggon, et al. (Eds.), Proceed. Oman D.P. (International Ocean Discovery Program), doi: 10.14379/OmanDP.proc.115.2020.

Kelemen P.B., Shimizu N. and Salters V.J.M., 1995a. Extraction of mid-ocean-ridge basalt from the upwelling mantle by focused flow of melt in dunite channels. Nature, 375: 747-753.

Khedr M.Z., Arai S., Python M. and Tamura A., 2014. Chemical variations of abyssal peridotites in the central Oman ophiolite: evidence of oceanic mantle heterogeneity. Gondw. Res., 25: 1242-1262.

Koepke J., Feig S.T., Berndt J., Neave D.A. and Oman D.P. Sci. Team, 2021. Wet magmatic processes during the accretion of the deep crust of the Oman Ophiolite paleoridge: Phase diagrams and petrological records. Tectonophysics, 817: 229051, doi: 10.1016/j.tecto.2021.229051.

Koga K.T., Kelemen P.B. and Shimizu N., 2001. Petrogenesis of the crust-mantle transition zone and the origin of lower crustal wehrlites in the Oman ophiolite. Geochem. Geophys. Geosyst., 2, doi: 10.1029/2000GC000132.

Laukert G., Von der Handt A., Hellebrand E., Snow J., Hoppe P. and Klugel A., 2014. High-pressure reactive melt stagnation recorded in abyssal pyroxenites from the ultraslow-spreading Lena Trough, Arctic Ocean. J. Petrol., 55: 427-458.

Le Mée L., Girardeau J. and Monnier C., 2004. Mantle segmentation along the Oman ophiolite fossil mid-ocean ridge. Nature, 432: 167-172.

Liang Y., 2003. Kinetics of crystal-melt reaction in partially molten silicates: 1. Grain scale processes. Geochem.Geophys. Geosyst., 4, doi:10.1029/2002GC000375.

Lippard S.J., Shelton A.W. and Gass I.G., 1986. The Ophiolite of Northern Oman. Geol. Soc. London Mem., 11: 178.

MacLeod C.J., Lissenberg C.J. and Bibby L.E., 2013. "Moist MORB" axial magmatism in the Oman ophiolite: The evidence against a mid-ocean ridge origin. Geology, 41: 459-462, doi: 10.1130/G33904.1.

Montigny R., Le Mer O. and Whitechurch H., 1988. K-Ar and $^{40}Ar/^{39}Ar$ study of metamorphic rocks associated with the Oman ophiolite: tectonic implications. Tectonophysics, 151: 345-362.

Morgan Z. and Liang Y., 2005. An experimental study of the kinetics of lherzolite reactive dissolution with applications to melt channel formation. Contrib. Miner. Petrol., 150: 369-385.

Morishita T. and Arai S., 2001. Petrogenesis of corundum-bearing mafic rock in the Horoman Peridotite Complex, Japan. J. Petrol., 42: 1279-1299.

Morishita T., Arai S., Gervilla F. and Green D.H., 2003. Closed system geochemical recycling of crustal materials in the upper mantle. Geochim. Cosmochim. Acta, 67: 303-310.

Nicolas A. and Boudier F., 1995. Mapping oceanic ridge segments in Oman ophiolite. J. Geophys, Res., 100: 6179-6197.

Nicolas A. and Prinzhofer A., 1982. Cumulative or residual origin for the transition one in ophiolites: Structural evidence. J. Petrol., 24: 188-206.

Nicolas A., Boudier F., Ildefonse B. and Ball E., 2000. Accretion of Oman ophiolite and United Emirates ophiolite: Discussion of a new structural map. Mar. Geophys. Res., 21: 147-179.

Nicolle M., Jousselin D., Reisberg L., Bosch D. and Stephant A., 2016. Major and trace element and Sr and Nd isotopic results from mantle diapirs in the Oman ophiolite: Implications for off-axis magmatic processes. Earth Planet. Sci. Lett., 437: 138-149, doi: 10.1016/j.epsl.2015.12.005.

Nimis P. and Taylor W.R., 2000. Single clinopyroxene thermobarometry for garnet peridotites. Part I. Calibration and testing of a Cr-in-Cpx barometer and an enstatite-in-Cpx thermometer. Contrib. Miner. Petrol., 139: 541-554.

Pearce J.A., Alabaster T., Shelton A.W. and Searle M.P., 1981. The Oman Ophiolite as a Cretaceous Arc-Basin Complex: evidence and implications. Philosoph. Transcr. Royal Soc. London, 299-317, doi: 10.1098/rsta.1981.0066.

Python M. and Ceuleneer G., 2003. Nature and distribution of dykes and related melt migration structures in the mantle section of the Oman ophiolite. Geochem. Geophys. Geosyst., 4(7): 8612, doi:10.1029/2002GC000354.

Python M., Ceuleneer and G., Arai S., 2008. Chromian spinels in mafic-ultramafic mantle dykes: evidence for a two-stage melt production during the evolution of the Oman ophiolite. Lithos, 106: 137-154.

Rabinowicz M., Ceuleneer G. and Nicolas A., 1987. Melt segregation and flow in mantle diapirs below spreading centres: evidence from the Oman ophiolite. J. Geophys. Res., 92: 3475-3486.

Rampone E., Borghini G. Basch V., 2020. Melt migration and melt-rock reaction in the Alpine-Apennine peridotites: Insights on mantle dynamics in extending lithosphere. Geosci. Front., 11: 151-166, doi: 10.1016/j.gsf.2018.11.001.

Rioux M., Bowring S., Kelemen P., Gordon S., Dudás F. and Miller R., 2012. Rapid crustal accretion and magma assimilation in the Oman-U.A.E. ophiolite: high precision U-Pb zircon geochronology of the gabbroic crust. J. Geophys. Res., 117: B07201, doi: 10.1029/2012JB009273.

Rioux M., Bowring S., Kelemen P., Gordon S., Miller R. and Dudás F., 2013. Tectonic development of the Samail ophiolite: high-precision U-Pb zircon geochronology and Sm-Nd isotopic constraints on crustal growth and emplacement. J. Geophys. Res. Solid Earth, 118: 2085-2101, doi: 10.1002/jgrb.50139.

Rospabé M., Benoit M., Ceuleneer G., Hodel F. and Kaczmarek M-A., 2018. Extreme geochemical variability through the dunitic transition zone of the Oman ophiolite: Implications for melt/fluid-rock reactions at Moho level beneath oceanic spreading centers. Geochim. Cosmochim. Acta, 234: 1-23, doi: 10.1016/gca.2018.05.012.

Salters V.J.M., Stracke A., 2004. Composition of the depleted mantle. Geochemistry, Geophysics, Geosystems, 5: Q05B07, doi: 10.1029/2003GC000597.

Sani C., Sanfilippo A., Ferrando C., Peyve A.A., Skolotnev S.G., Muccini F., Zanetti A., Basch V., Palmiotto C., Bonatti E. and Ligi M., 2020. Ultra-depleted melt refertilization of mantle peridotites in a large intra-transform domain (Doldrums Fracture Zone; 7-8°N, Mid-Atlantic Ridge). Lithos, 374-375: 105698, doi: 10.1016/j.lithos.2020.105698.

Stracke A. Salters V.J.M. and Sims K.W.W., 2000. Assessing the presence of garnet-pyroxenite in the mantle sources of basalts through combined hafnium-neodymium-thorium isotope systematics. Geochem. Geophys. Geosyst., 1, doi: 10.1029/1999GC000013.

Takazawa E., Frey F.A., Shimizu N., Saal N. and Obata M., 1999. Polybaric petrogenesis of mafic layers in the Horoman peridotite complex, Japan. J. Petrol., 40: 1827-1831.

Takazawa E., Okayasu T. and Satoh K., 2003. Geochemistry and origin of the basal lherzolites from the northern Oman ophiolite (northern Fizh block). Geochem. Geophys. Geosyst., 4.

Taylor W.R., 1998. An experimental test of some geothermometer and geobarometer formulations for upper mantle peridotites with application to the thermobarometry of fertile lherzolite and garnet websterite. N. Jahrb. Miner. Abh, 172: 381-408.

Van Acken D., Becker H., Walker R.J., McDonough W.F., Wombacher F., Ash R.D. and Piccoli P.M., 2010. Formation of pyroxenite layers in the Totalp ultramafic massif (Swiss Alps)-Insights from highly siderophile elements and Os isotopes. Geochim. Cosmochim. Acta, 74: 661-683.

Warren J.M., 2016. Global variations in abyssal peridotite compositions. Lithos, 248-251: 193-219, doi: 10.1016/j.lithos.2015.12.023.

Yamasaki T., Maeda J. and Mizuta T., 2006. Geochemical evidence in clinopyroxenes from gabbroic sequence for two distinct magmatism in the Oman ophiolite. Earth Planet. Sci. Lett., 251: 52-65, doi: 10.1016/j.epsl.2006.08.027.

Yoshikawa M., Python M., Tamura A., Ari S., Takazawa E., Shibata T., Ueda A. and Sato T., 2015. Melt extraction and metasomatism recorded in basal peridotites above the metamorphic sole of the northern Fizh massif, Oman ophiolite. Tectonophysics, 650: 53-64, doi: 10.1016/j.tecto.2014.12.004.

Yu S., Xu Y., Ma J., Zheng Y., Kuang Y., Hong L., Ge W. and Tong L., 2010. Remnants of oceanic lower crust in the subcontinental lithospheric mantle: trace element and Sr-Nd-O isotope evidence from aluminous garnet pyroxenite xenoliths from Jiaohe, Northeast China. Earth Planet. Sci. Lett., 297: 413-422.

Received, June 6, 2022
Accepted, September 30, 2022
First published online, October 7, 2022